Structure and dielectric studies of (1-x)Ba$_{0.06}$(Na$_{0.5}$Bi$_{0.5}$)$_{0.94}$TiO$_3$-xBa(Fe$_{0.5}$Nb$_{0.5}$)O$_3$ lead-free ceramics

Sumit K. Roy[1], Satyendra N. Singh[2], Sanat K. Mukherjee[3], Kamal Prasad[4,*]

[1]Department of Physics, St. Xavier's College, Ranchi 834001, India

[2]University Department of Physics, Ranchi University, Ranchi, 834008, India

[3]Department of Physics, BIT, Mesra, Ranchi 835215, India

[4]University Department of Physics, T.M. Bhagalpur University, Bhagalpur, 812007, India

Abstract

In this work, the effects of Ba(Fe$_{0.5}$Nb$_{0.5}$)O$_3$ (BFN) addition on the structure and dielectric behaviour of Ba$_{0.06}$(Na$_{0.5}$Bi$_{0.5}$)$_{0.94}$TiO$_3$ (BNBT) ceramics have been reported. The lead-free (1-x)BNBT-xBFN (where 0 ≤ x ≤ 1.0) solid-solutions were synthesized by traditional ceramics fabrication technique and sintered at temperatures up to 1325 °C. The X-ray diffraction peaks of the compounds of the entire series were indexed. It is found that the crystal structure of the obtained solid solutions changed from rhombohedral (R3c) to cubic (Pm3m) with an increase in BFN content. The Fourier transformed infrared and Raman spectra also confirmed the formation of solid-solutions. SEM studies were carried out to evaluate the purity and microstructure of the fabricated ceramics. The dependence of phase transition broadening, phase transition temperature and dielectric parameters with compositional changes were also studied.

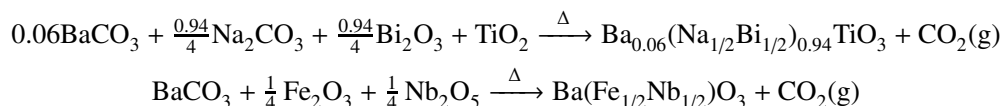*Keywords: perovskites, lead-free ceramics, microstructure, dielectric constant, impedance*

I. Introduction

Lead-based ceramics are widely used in the electronics industry for various electronic, microelectronic, electro-optic and magneto-electric devices [1]. Most of the products end up in a landfill within a few months or years as they have a short service life. Attempts to recycle lead in electronic products had mostly been unsuccessful [2]. The disposed lead in the environment has subsequent effects on the ecosystem which needs to be addressed. Most leading electronic manufacturers have prioritized their search for alternatives to lead-containing ceramics. In recent years, complex perovskites with Fe as one of the components having nominal chemical formula A(Fe$_{1/2}$B$_{1/2}$)O$_3$ (A = Ba, Sr and Ca; B = Nb, Ta and Sb) have lured researchers because of their giant dielectric (10^3–10^5) response over a wide temperature and frequency interval [3–7]. Reaney *et al.* [8] for the first time reported the structural studies of Ba(Fe$_{1/2}$Na$_{1/2}$)O$_3$ (BFN). Saha and Sinha [9] reported

that BFN possesses a partially disordered perovskite structure exhibiting ferroelectric relaxation, characterized by a broad dielectric transition. Raevski *et al.* [4] reported that the high values of the dielectric permittivity in BFN and similar ceramics can be accounted to the Maxwell-Wagner mechanism. Afterwards, continuous efforts had been made to study the dielectric behaviour of BFN [5,10–14]. Ke *et al.* [15] demonstrated that with suitable sintering conditions the value of dielectric permittivity (ε_r) of BFN can be increased above 10^5. The microwave synthesis of BFN powder and its dielectric properties had been studied by Charoenthai *et al.* [16] for the first time by microwave synthesis technique. They obtained pure perovskite phase having cubic symmetry with average particle size in the submicron range. The reported dielectric constant and dielectric loss at 300 °C and 1 kHz was ~30000 and 0.6. Eitssayeam *et al.* [17] studied the ferroelectric and pyroelectric properties of 0.8PbZr$_{0.52}$Ti$_{0.48}$O$_3$-0.2BaFe$_{0.5}$Nb$_{0.5}$O$_3$ ceramic system and quoted the remanent polarization and coercive field of 0.8PZT-0.2BFN ceramics to be 21 μC/cm^2 and 6.4 kV/cm, respectively. Chung *et al.* [18] studied the fluctuations in the dielectric behaviour of BFN

*Corresponding author: tel: +91 641 2501699,
e-mail: *Prasad_k@tmbuniv.ac.in, k.prasad65@gmail.com*

ceramics upon the introduction of bismuth. When Bi doping level was below 6 mol% single-phase monoclinic perovskite structure was obtained and above 6 mol% the ceramic structure changed to tetragonal symmetry. Bi doped BFN ceramics showed the dielectric relaxation properties and the giant dielectric constant response by the boundary-layer mechanism. Lead-free pseudo-binary compounds, $(1-x)Ba(Fe_{1/2}Nb_{1/2})O_3$-$xBaTiO_3$ ($0 \leq x \leq 1$), were studied by Bhagat *et al.* [19]. They reported that the incorporation of $BaTiO_3$ significantly reduced the dielectric loss and improved the frequency and temperature stability of the dielectric properties of $Ba(Fe_{1/2}Nb_{1/2})O_3$. Dielectric and Mössbauer spectra studies of BFN ceramics with monoclinic and cubic perovskite structures were undertaken by Raevski *et al.* [20]. They reported that high value of the dielectric constant in both structures is determined not by intrinsic ferroelectric properties, but rather by extrinsic contribution due to the polarization of the Maxwell-Wagner type at low temperatures and/or relaxation contributed by the oxygen vacancies at high temperatures. In recent work, Li *et al.* [21] studied Al-substitution for Fe in $Ba(Fe_{0.5}Nb_{0.5})O_3$ ceramics. They observed that both pure BFN and Al doped BFN possess cubic crystal structure with $Pm3m$ (221) space group.

$$0.06BaCO_3 + \tfrac{0.94}{4}Na_2CO_3 + \tfrac{0.94}{4}Bi_2O_3 + TiO_2 \xrightarrow{\Delta} Ba_{0.06}(Na_{1/2}Bi_{1/2})_{0.94}TiO_3 + CO_2(g)$$

$$BaCO_3 + \tfrac{1}{4}Fe_2O_3 + \tfrac{1}{4}Nb_2O_5 \xrightarrow{\Delta} Ba(Fe_{1/2}Nb_{1/2})O_3 + CO_2(g)$$

A close observation of the periodic table and literature survey suggests that the most likely replacements for the lead-based materials having in mind the environmental factors are the Bi-based compounds [22,23]. Among the Bi-based systems, $(1-x)(Bi_{1/2}Na_{1/2})TiO_3$-$xBaTiO_3$ is considered to be one of the potential lead-free candidates for dielectric and/or piezoelectric applications. It exhibits a rhombohedral-tetragonal morphotropic phase boundary (MPB) around $0.06 \leq x \leq 0.08$ with noticeable piezoelectric, dielectric and electro-magnetic properties [24,25]. However, the non-lead pseudo-binary solid-solution of $Ba_{0.06}(Na_{1/2}Bi_{1/2})_{0.94}TiO_3$ and $Ba(Fe_{1/2}Nb_{1/2})O_3$ (abbreviated hereafter as BNBT-BFN) has not been investigated/reported by any research group and this is the motivation of our research work.

The aim of the present study is to investigate the effects of BFN addition on the various quantities of interest like the structural and dielectric properties of BNBT ceramics. It is very well established in the literature that the ionic radius of the doped/foreign cations and their mixed-valences are key parameters governing the electrical properties of the parent materials. Taking into account the various parameters, namely the tolerance factor, the charge balance and the Coulombic and strain interactions, transition metal Fe and Nb in $Ba(Fe_{1/2}Nb_{1/2})O_3$ are more likely to be incorporated into the B site of BNBT matrix since in this situation the involved degree of ionic

radii mismatch is the lowest [28]. Thus, the possible B-site substitution formula for the solid solution of $Ba_{0.06}(Na_{1/2}Bi_{1/2})_{0.94}TiO_3$ and $Ba(Fe_{1/2}Nb_{1/2})O_3$ is $Ba_{0.06+0.94x}Na_{0.47(1-x)}Bi_{0.47(1-x)}Fe_{0.5x}Nb_{0.5x}Ti_{(1-x)}O_3$.

In this work, (1-x)BNBT-xBFN ($0 \leq x \leq 1.0$) powders were synthesized by conventional solid-state reaction method, pressed and sintered up to 1325 °C. X-ray diffraction, scanning electron microscopy, FTIR, Raman spectroscopy and dielectric studies were used to characterize the samples. From all these experimentally obtained data the formation of the solid solution was confirmed and the effect of composition on the phase transition broadening and phase transition temperature were also analysed.

II. Experimental

The polycrystalline $Ba_{0.06}(Na_{1/2}Bi_{1/2})_{0.94}TiO_3$ and $Ba(Fe_{1/2}Na_{1/2})O_3$ powders were prepared separately by solid-state reaction technique using high purity (>99.9%) carbonates/oxides, i.e. $BaCO_3$, Na_2CO_3, Bi_2O_3, TiO_2 and Nb_2O_5. Following thermochemical reactions were carried out in an air atmosphere at 1140 °C and 1300 °C, respectively:

The completion of the reactions and the formation of desired compounds were confirmed by X-ray diffraction technique. BNBT was then mixed with varying amount of BFN. Wet mixing was carried out with methanol as the medium for homogeneous mixing. A series of $(1-x)Ba_{0.06}(Na_{1/2}Bi_{1/2})_{0.94}TiO_3$-$xBa(Fe_{1/2}Nb_{1/2})O_3$ (where $x = 0, 0.05, 0.10, 0.25, 0.50, 0.75, 0.90, 0.95$ and 1.0) samples were compressed into thin (~1.5 mm) cylindrical disks with an applied uniaxial pressure of 5 tons. The prepared samples were finally sintered at temperatures between 1180 °C ($x = 0$) and 1325 °C ($x = 1.0$) for 4 h except for $x = 0.50$. Great difficulty was encountered in sintering of the 0.5BNBT-0.5BFN solid solution. The sintering temperature of this composition (1150 °C) was less than for the composition preceding it as well as succeeding it. In addition, any slight variation from this temperature resulted in melting of the solid solution.

The sintered (1-x)BNBT-xBFN ($0 \leq x \leq 1.0$) pellets were characterized by X-ray diffraction technique at room temperature, using diffractometer (X'pert PRO, PanAlytical) with CuKα radiation ($\lambda = 1.5406$ Å) and over a wide range of Bragg angles from 10° to 70°.

The Fourier transformed infrared (FTIR) spectra of (1-x)BNBT-xBFN ($0 \leq x \leq 1.0$) samples were recorded in the transmission mode with Alpha-T Bruker FTIR spectrophotometer in the range of 500–4000 cm^{arg}-1.

The sintered pellets were polished properly to ensure the parallel surfaces. The circular faces of the pellets were coated with silver paste and fired at 500 °C for
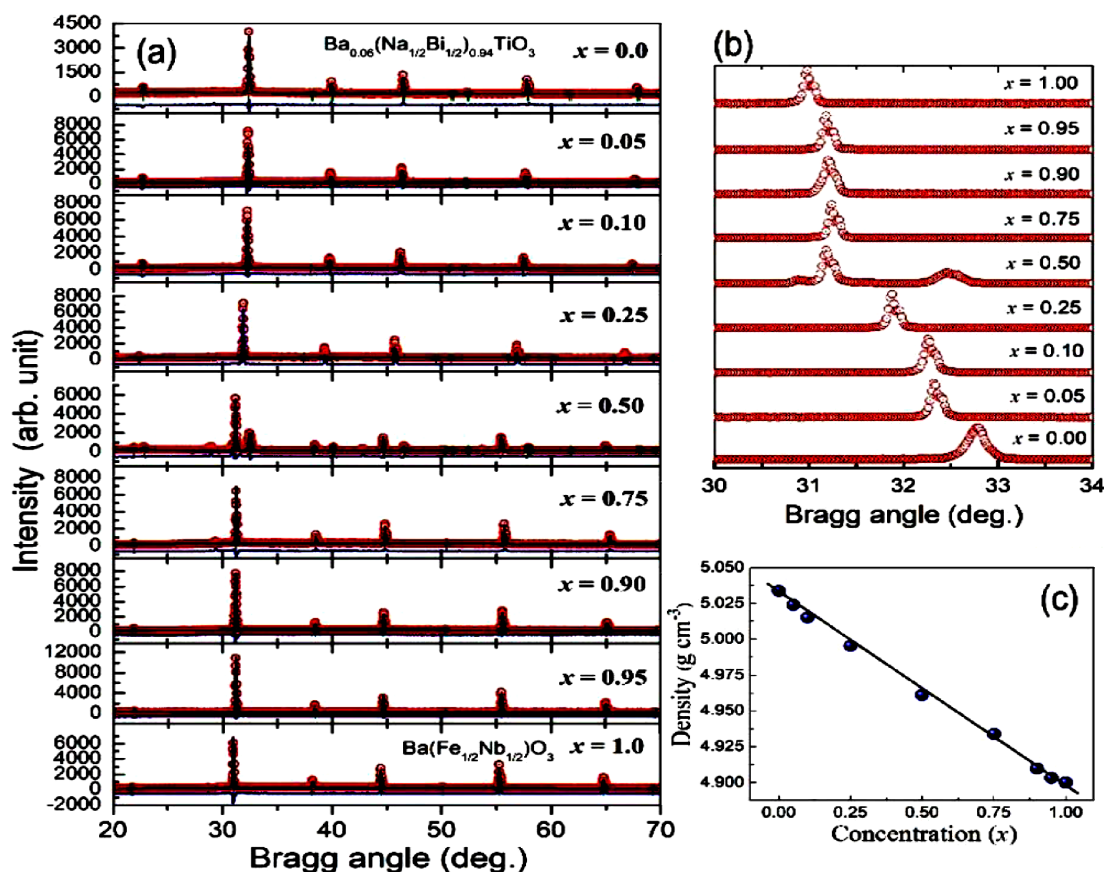
Figure 1. Rietveld refined XRD patterns (a), XRD patterns of the selected regions - 2θ range: 30°–34° (b) and measured density of Ba$_{0.06}$(Na$_{1/2}$Bi$_{1/2}$)$_{0.94}$TiO$_3$-Ba(Fe$_{1/2}$Nb$_{1/2}$)O$_3$ ceramics (c) (symbols represent the observed data points and the solid lines their Rietveld fit)

30 min. The metal coating acts as the electrodes for the electrical measurements. The frequency (1 Hz–1 MHz) and temperature (50–400 °C) dependent dielectric constant (real and imaginary parts) of the different compositions were measured using a computer-controlled Alpha high-resolution dielectric analyser (NOVOCONTROL Technologies, GmbH & Co. KG, Germany). The temperature was varied at a rate of 2 °C/min.

III. Results and discussion

Figure 1a displays the observed, calculated and difference profiles of Rietveld refined XRD patterns of the sintered (1-x)BNBT-xBFN ceramics having x = 0.00, 0.05, 0.10, 0.25, 0.50, 0.75, 0.90, 0.95 and 1.00. All the samples except x = 0.50 are a pure phase with a perovskite structure. It has been reported that rhombohedral-tetragonal symmetry exists at MPB composition in Ba$_{0.06}$(Na$_{1/2}$Bi$_{1/2}$)$_{0.94}$TiO$_3$ [24,25] and the space group $R3c$ is found to fit well the X-ray diffraction pattern [26]. The crystal structure of Ba(Fe$_{1/2}$Nb$_{1/2}$)O$_3$ at room temperature is reported to have cubic symmetry with $Pm3m$ space group [21]. It could be seen that diffraction peaks of Ba$_{0.06}$(Na$_{1/2}$Bi$_{1/2}$)$_{0.94}$TiO$_3$ (x = 0) and Ba(Fe$_{1/2}$Nb$_{1/2}$)O$_3$ (x = 1) are consistent with the earlier reports [21,27]. The shift in the peak positions and changes in intensities of the peaks can be noticed

(Fig. 1b) with the addition of BFN to BNBT matrix. The room temperature crystal structure of the samples gradually changed from rhombohedral-tetragonal to cubic symmetry with increasing x. The crystal structure of the samples with $x \leq 0.25$ was found to be rhombohedral ($R3c$) and that with higher BFN content ($x \geq 0.75$) were found to be cubic ($Pm3m$). The XRD pattern of solid-solution with composition x = 0.50 was found to contain the peaks corresponding to both tetragonal as well as cubic symmetry, revealing a mixed phase with 53% contribution from rhombohedral-tetragonal phase (space group: $R3c$) and 47% contribution from cubic phase (space group: $Pm3m$) as evident from the Rietveld refinement.

Figure 2 shows the SEM micrographs of the cross section of the BNBT-BFN ceramics after sintering. The SEM images reveal that grains are distributed throughout the samples with no or very few voids, indicating that the sintered samples had attained high density (5.03 g/cm^3 for x = 0 to 4.78 g/cm^3 for x = 1.0). Polycrystalline grains with grain sizes ranging from 3–10 μm were found for the chosen compositions. The substitution of Fe/Nb for Ti led to an obvious change in the grain shape and size. The average grain size for the BNBT sample is found to be ≈3 μm. As the substitution level of Fe/Nb increased to 0.25, the grains became significantly larger (6 μm) and grew into granular shapes

Table 1. The crystal data and refinement factors of $(1-x)Ba_{0.06}(Na_{1/2}Bi_{1/2})_{0.94}TiO_3$-$xBa(Fe_{1/2}Nb_{1/2})O_3$ ceramics obtained from X-ray powder diffraction data at room temperature (R - rhombohedral and C - cubic)

Parameters	$x = 0.0$	$x = 0.05$	$x = 0.10$	$x = 0.25$	$x = 0.50$		$x = 0.75$	$x = 0.90$	$x = 0.95$	$x = 1.0$
Crystal system	R	R	R	R	R + C		C	C	C	C
Space group	$R3c$	$R3c$	$R3c$	$R3c$	$R3c$	$Pm3m$	$Pm3m$	$Pm3m$	$Pm3m$	$Pm3m$
a (Å)	5.518	5.534	5.552	5.672	5.525	4.059	4.029	4.047	4.053	4.056
b (Å)	5.518	5.534	5.552	5.672	5.525	4.059	4.029	4.047	4.053	4.056
c (Å)	13.513	13.509	13.617	13.50	13.48	4.059	4.029	4.047	4.053	4.056
V (Å^3)	356	358.39	363.62	376.45	356.43	66.89	65.43	66.30	66.6	66.77
R_{exp}	6.4	6.4	6.39	6.35	6.23		6.22	6.12	5.84	6.27
R_p	8.3	9.5	12.47	15.82	10.06		10.16	7.91	14.49	10.94
R_{wp}	10.2	13.5	15.38	28.115	13.81		12.95	10.39	17.2	13.70
R_B	5.22	12.05	9.25	27.31	2.82	2.96	13.16	6.3	6.26	19.44
χ^2 (GOF)	2.59	4.34	5.78	19.59	4.91		4.32	2.87	8.65	4.76
D	1.6	0.58	0.35	0.119	0.17		0.20	0.5	0.13	0.16
c/a	2.45	2.44	2.45	2.38	2.44	1.0	1.0	1.0	1.0	1.0
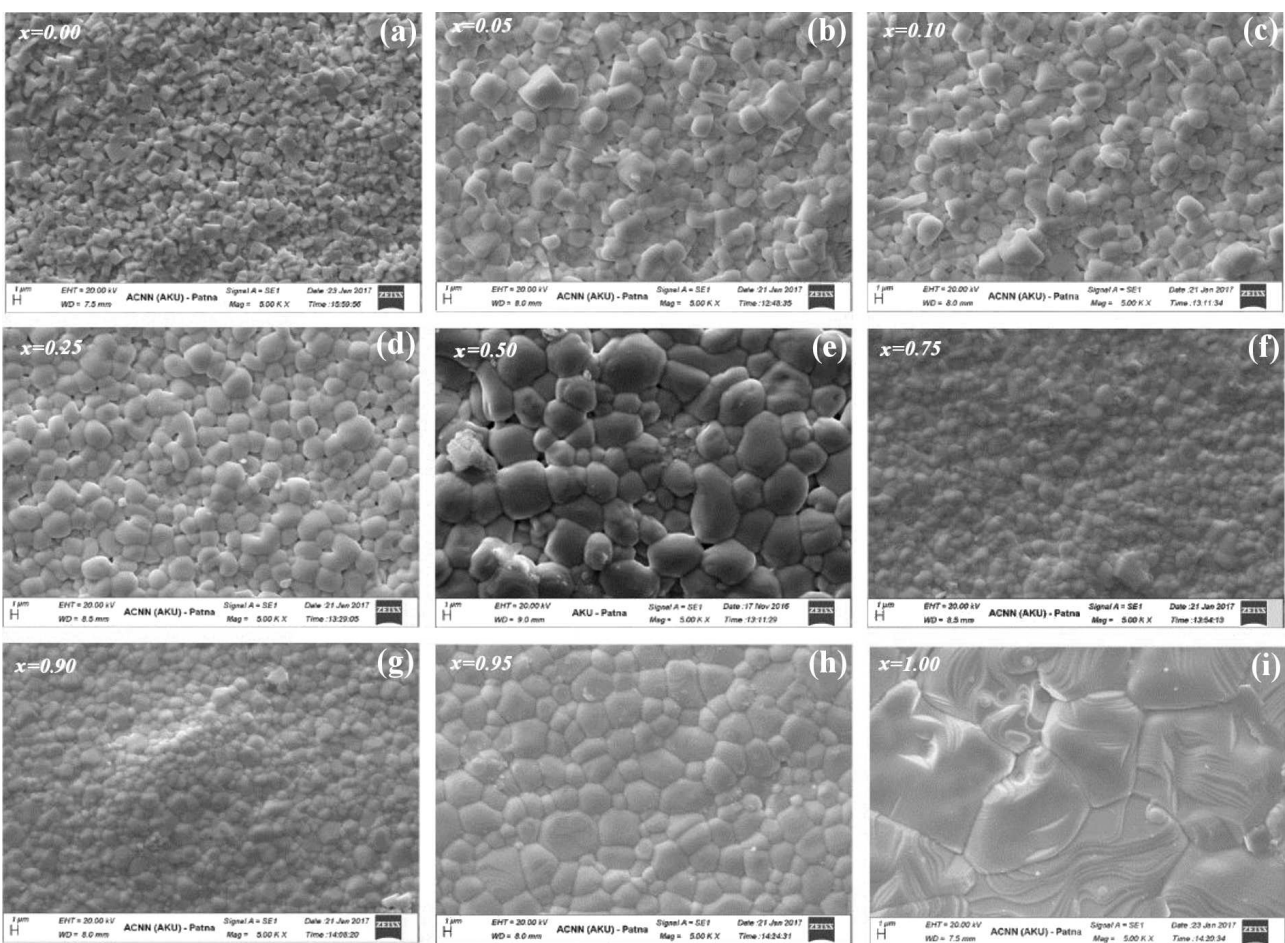
Figure 2. Scanning electron micrographs of $(1-x)Ba_{0.06}(Na_{1/2}Bi_{1/2})_{0.94}TiO_3$-$xBa(Fe_{1/2}Nb_{1/2})O_3$ ceramics: a) $x = 0$, b) $x = 0.05$, c) $x = 0.10$, d) $x = 0.25$, e) $x = 0.50$, f) $x = 0.75$, g) $x = 0.90$ h) $x = 0.95$ and i) $x = 1.00$

with grain boundaries slightly blurred as compared to the lower compositions. The grain size continuously increases with increase in BFN content (x) and there are two possible reasons. The first one could be the difference in ionic radii, i.e. the ionic radius of Fe and Nb are greater than the ionic radius of Ti which they replace [$r(Fe_{VI}^{3+})$ = 0.645 Å, $r(Nb_{VI}^{5+})$ = 0.69 Å and $r(Ti_{VI}^{4+})$ = 0.605 Å]. The second possible reason is that this growth is due to the Ostwald ripening, a thermo-

dynamically driven process where crystal growth takes place by a dissolution-precipitation mechanism, usually when a secondary phase is present, to attain a lower value of chemical potential as well as the Gibbs free energy [29]. The Ostwald ripening could be recognised in the samples with composition having $x = 0.50$ where a mixed phase was confirmed by XRD. The larger average grain size of 10 μm has the sample with $x = 1.00$.

Figure 3 shows the FTIR spectra of the BNBT–BFN

ceramics in the mid-infrared region. Peaks corresponding to the metal-oxygen bond can confirm the formation of a perovskite structure [24]. In the unit cell of the perovskite BNBT, Ba, Na, and Bi are at the A-site, Ti at the B-site and oxygen at the face centre. Reduced masses of Bi–O, Ba–O, Ti–O and Na–O are in decreasing order hence their metal oxide (M–O) bonds have their characteristic wavenumbers in increasing order. However, there could be variations in the above-mentioned trend owing to degenerate infrared-active vibrations of a particular M–O bond. Considering these facts, it can be inferred that in the FTIR spectra of the BNBT, a sharp peak near $610 \, cm^{-1}$ represents the Ti–O stretching mode [25], an intense band at $642 \, cm^{-1}$ may be accredited to the bonding of either Ba–O or Bi–O and a comparatively weak band at $842 \, cm^{-1}$ may be accredited to Na–O bond. Earlier reports suggest that the peaks corresponding to Ti–O stretching mode and TiO_6 polyhedron absorb near $395 \, cm^{-1}$ [25] and $410 \, cm^{-1}$, not present in the spectrum as these are beyond the recorded range [26,27]. Further, with the increase of BFN content (x), the peak at $642 \, cm^{-1}$ becomes narrower, decreases in intensity and shifts towards the lower wavenumber side. The narrowing of the peak may be attributed to the increasing number of chemical environments. The two dominant peaks at $642 \, cm^{-1}$ and $842 \, cm^{-1}$ coalesce
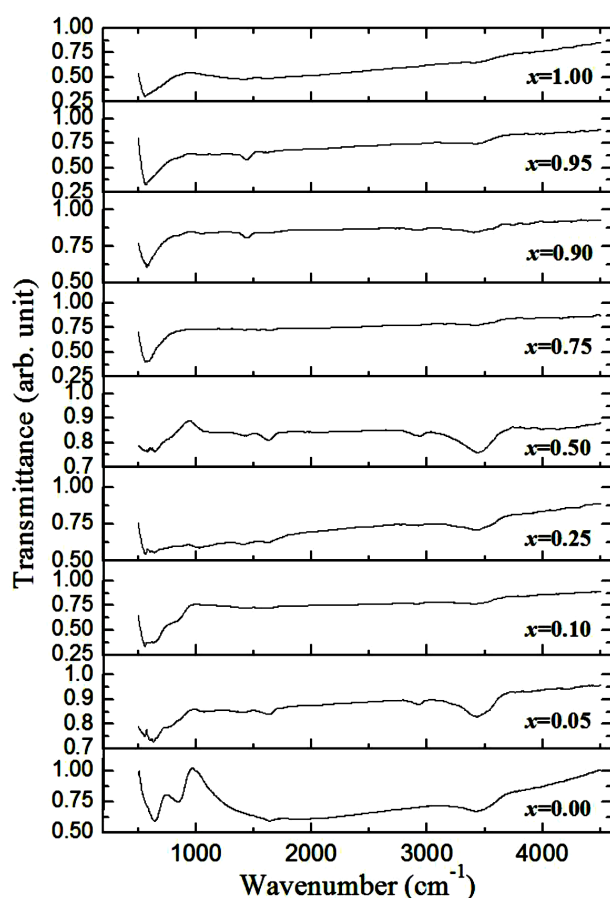
to form a single peak around $573 \, cm^{-1}$ for $x = 0.75$. The peak at $573 \, cm^{-1}$ may be attributed to the Fe–O stretching and bending vibration which is characteristic of octahedral FeO_6 groups in the perovskite compounds [28]. The peaks for $x = 0.90$ again become narrow and sharp which may be a confirmation of weak intermolecular interactions due to a decrease in a number of chemical environments. All the compounds contain weak band at $2800–2900 \, cm^{-1}$ which correspond to carbonate groups, may be due to atmospheric CO_2. During palletisation with KBr some water molecules are adsorbed from the atmosphere and hence H–O–H bending and O–H stretching modes of vibration at 1639 and $3443 \, cm^{-1}$ are also present for the entire series of BNBT-BFN ceramic system.

Figure 4 shows the first-order Raman spectra of the sintered $(1\text{-}x)$BNBiT-xBFN ceramics with $x = 0.00$, 0.05, 0.10, 0.25, 0.50, 0.75, 0.90, 0.95 and 1.00. The peaks of BNBT which were expected to be Lorentzian in line-shape were found to be Gaussian line-shape [30]. Numbers 133.3 (19.2), 281.3 (53.4), 536.2 (49.7), 615.3 (28.11) and 799.4 (79.2) cm^{-1} in graphs mark the peak position with FWHM in parenthesis. Gaussian peak profile observed in the Raman spectra of BNBT may be attributed to the particle size distribution in the sample [30]. Acute and multiple Lorentzian peaks were observed in BFN in contrast to BNBT. As shown in Fig. 4a, no new peaks are observed with increasing BFN content (x), thereby indicating the formation of solid solutions of BNBT-BFN and consequently the absence of formation of any new phase. Since the Raman peaks of BFN differ significantly from that of BNBT (Fig. 4b), the evolution of the structural changes of BNBT-BFN solid solutions due to change in composition, can be correlated with XRD and dielectric data. Also, the Raman bands are quite broad. Broad Raman bands are an indicator of cation disorder at the coordinated sites and overlapping of Raman modes [31].

3.1. Dielectric properties

Temperature dependences of the dielectric constant and loss for the BNBT-BFN ceramics at 1 kHz, 10 kHz and 100 kHz are shown in Figs. 5 and 6. The phase transition in the samples with lower BFN content ($0 \leq x \leq 0.25$) is diffuse which becomes sharp with the predomination of the cubic phase ($x \geq 0.75$). The ceramics with lower BFN content have two dielectric anomalies at T_d (depolarization temperature) and T_m (temperature corresponding to the maximal dielectric constant) as observed from Fig. 5, whereas only one significant phase transition is noted in the sample with higher BFN content ($x \geq 0.50$). With the increase in BFN concentration, the phase transition at first becomes more diffuse till $x = 0.25$. The widening of the ferroelectric phase transition in solid solution, in which similar crystallographic points are arbitrarily occupied by different types of ions, is attributed to the fluctuations in composition [32]. The phase transition broadening becomes an ex-
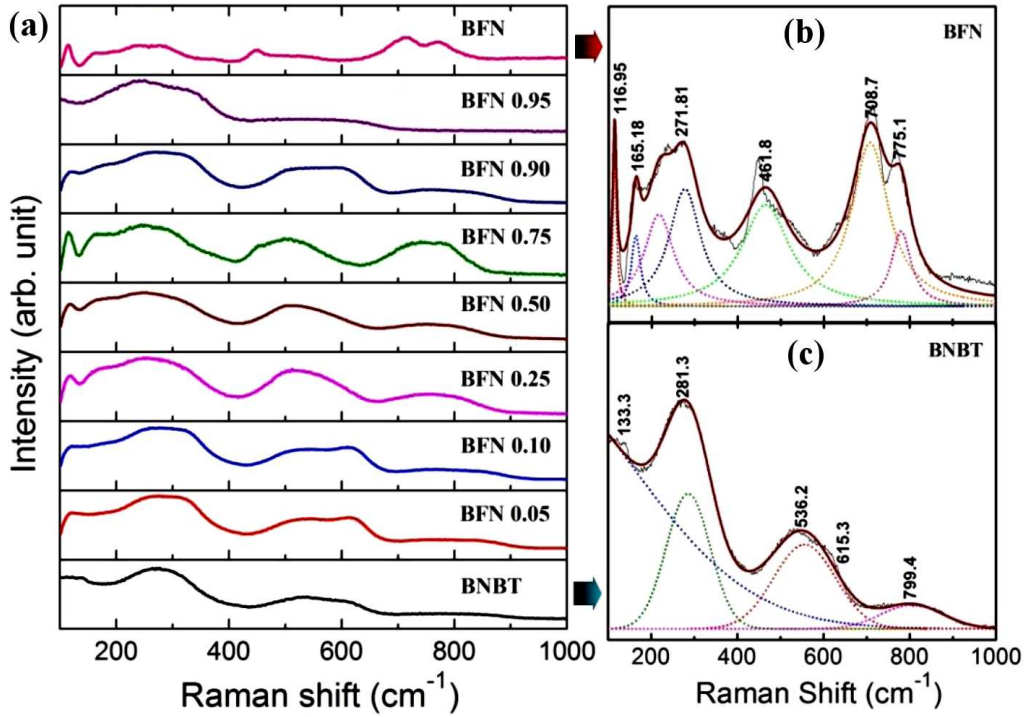

Figure 3. FTIR spectra of
$(1\text{-}x)$Ba$_{0.06}$(Na$_{1/2}$Bi$_{1/2}$)$_{0.94}$TiO$_3$-xBa(Fe$_{1/2}$Nb$_{1/2}$)O$_3$ ceramics at
room temperature

Figure 4. Raman (1-*x*)Ba$_{0.06}$(Na$_{1/2}$Bi$_{1/2}$)$_{0.94}$TiO$_3$-*x*Ba(Fe$_{1/2}$Ta$_{1/2}$)O$_3$ ceramics along with the Raman spectra of Ba$_{0.06}$(Na$_{1/2}$Bi$_{1/2}$)$_{0.94}$TiO$_3$ and Ba(Fe$_{1/2}$Nb$_{1/2}$)O$_3$ as well as their fitted peaks with Gaussian components and deconvoluted with Lorentzian components

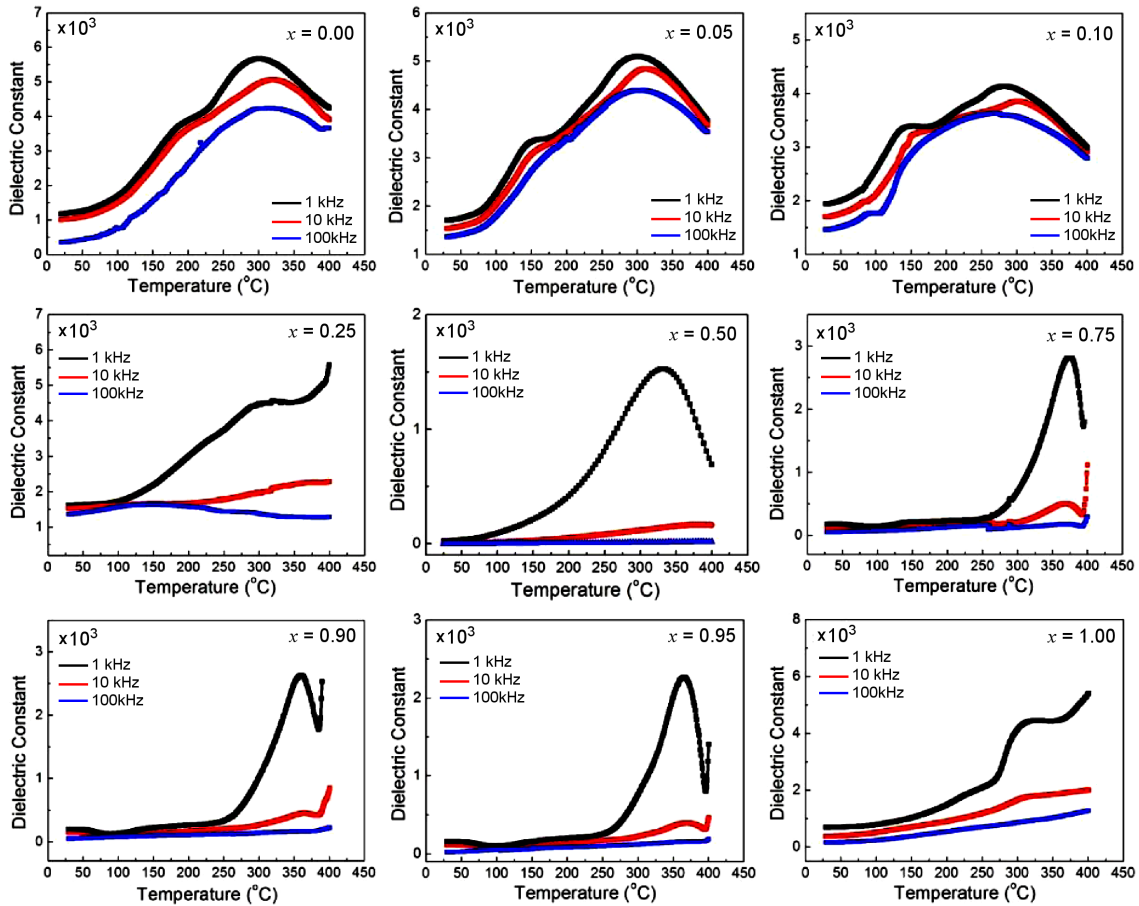**Figure 5. Temperature dependence of the dielectric constant of Ba$_{0.06}$(Na$_{1/2}$Bi$_{1/2}$)$_{0.94}$TiO$_3$-Ba(Fe$_{1/2}$Nb$_{1/2}$)O$_3$ ceramics at 1 kHz, 10 kHz and 100 kHz**
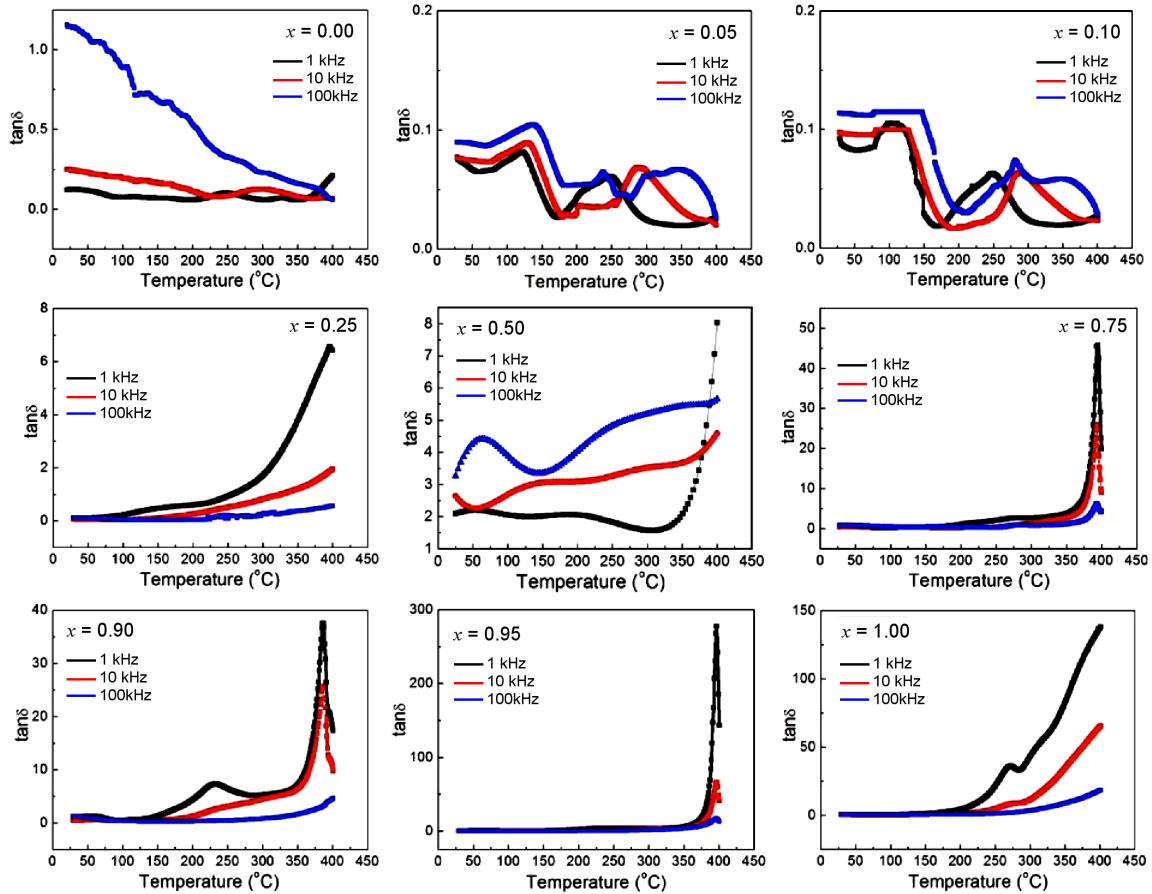
Figure 6. Temperature dependence of the loss tangent of Ba$_{0.06}$(Na$_{1/2}$Bi$_{1/2}$)$_{0.94}$TiO$_3$-Ba(Fe$_{1/2}$Nb$_{1/2}$)O$_3$ ceramics at 1 kHz, 10 kHz and 100 kHz

plicit function of the composition only when the long-range cooperative interactions between ions are weak enough. Thus, the substitution of Ti^{4+} with Fe^{3+} or Nb^{5+} ions into the B site of BNBT matrix seems to weaken the long-range cooperative forces between the B site ions, causing the composition fluctuation effective for the phase transition broadening. Hence, diffuse ferroelectric phase transition for $0 \leq x \leq 0.25$ could be due to the convergence of a large number of local ferroelectric phase transitions, which are caused by fluctuations in the local composition [31]. In addition to the effects on short-range forces, a direct long-range interaction between ions can originate from the local permanent electric dipoles with random orientations due to ion pairs (Fe^{3+},Ti^{4+}), (Fe^{3+},Nb^{5+}), (Ti^{4+},Nb^{5+}) etc. arranged together in the neighbouring B positions [32]. This causes an additional disturbance to the long-range cooperative interactions in crystals and may be responsible for a rapid phase transition broadening with an increase in the amount of BFN. Again, when BFN content is higher than 75% the phase transition broadening reduces due to the strengthening of long-range cooperative forces.

With the inclusion of BFN into BNBT matrix, the phase transition temperature displaces towards the higher temperature and attain its maximum for the composition with $x = 0.75$. The room temperature dielec-

tric constant (ε_{RT}), dielectric constant at the Curie temperature (ε_{max}) and loss tangent (tanδ) all have their maximal values for the composition with $x = 0.50$ at 1 kHz and they are 1197, 1.54×10^6 and 2.12, respectively (Fig. 7). The colossal dielectric constant near $x = 0.50$ may be attributed to various factors. The interaction of local permanent electric dipoles viz. (Fe^{3+},Ti^{4+}), (Fe^{3+},Nb^{5+}), (Ti^{4+},Nb^{5+}) etc., with random orientations is weak so the dipoles get easily polarized and the sample possesses higher magnitudes of dielectric constant under external alternating electric field [32]. The domain wall vibration is also one contributing component
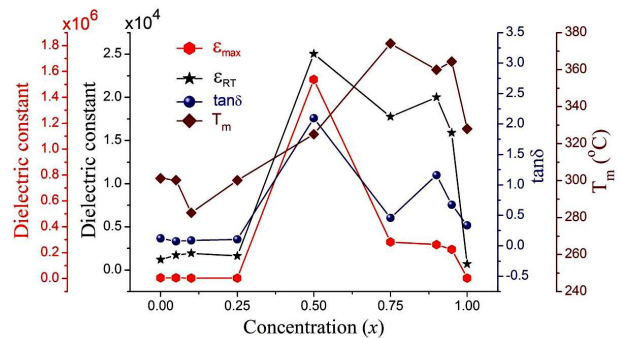

Figure 7. Compositional dependence of dielectric parameters of Ba$_{0.06}$(Na$_{1/2}$Bi$_{1/2}$)$_{0.94}$TiO$_3$-Ba(Fe$_{1/2}$Nb$_{1/2}$)O$_3$ ceramics at 1 kHz

to the dielectric constant (which is also called orientational polarization). The other contributing component is ionic polarization. If some of the Nb^{5+} ions substitute Ti^{4+} ions, cation vacancies may be created to maintain charge neutrality [33]. These cation vacancies may increase the ionic polarisation and in turn, contribute to the dielectric constant. A grain boundary is thought to have a lower dielectric constant than the ferroelectric grain, as dipoles within the grain boundary are more randomly oriented as compared to the grains, so with increasing grain size, the fraction of grain boundary volume decreases and the corresponding ceramics dielectric constant increases. For the series $(1-x)$BNBiT-xBFN samples with $x = 0.00, 0.10, 0.25, 0.50, 0.75, 0.90$ and 1.00, grain size is the largest for $x = 0.50$ and in accordance with the above theory dielectric constant is also maximal for $x = 0.50$. The similar kind of increment in dielectric constant due to the increase in grain size is explained by Lin *et al.* [34] by modifying Ginsburg-Landau-Devonshire thermodynamic theory. It is also a proven fact that any sample which possesses a spatial variation of charge density contributes to the dielectric susceptibility of a medium. The colossal dielectric constant near $x = 0.50$ at lower frequencies arises from intrinsically formed heterogeneous regions within the sample which represent a kind of Maxwell Wagner polarization effects. This agrees with the SEM micrograph as this composition marks the beginning of the Ostwald ripening after which the smaller crystals coalesce to form a bigger crystal. With $x \geq 0.75$ the dielectric response again decreases as the interaction between the local dipoles increases and the strong local interaction reduces the average polarization of the samples.

IV. Conclusions

Lead-free $(1-x)$Ba$_{0.06}$(Na$_{1/2}$Bi$_{1/2}$)$_{0.94}$TiO$_3$-xBa(Fe$_{1/2}$Nb$_{1/2}$)O$_3$; $0 \leq x \leq 1.0$ ceramics were prepared successfully following an industrially viable solid-state reaction technique. The Rietveld refinement of XRD data indicated that each composition of the series except $x = 0.50$ is a pure phase with perovskite structure. The composition with $x = 0.50$ was found to have a mixed phase of tetragonal and cubic symmetry, where 53% contribution comes from rhombohedral-tetragonal phase and 47% contribution comes from the cubic phase. As the substitution level of Fe/Nb (i.e. x) is increased the average grain size get increased from ~3 μm to 10 μm. The origin for the increment in grain size could be pinned down to the fact that ionic radius of Fe and Nb are greater than the ionic radius of Ti which they replace and to the Ostwald ripening. The grain shape changed from cuboidal like grains to granular like grains. The phase transition with lower BFN amount ($0 \leq x \leq 0.25$) is diffuse which becomes sharp as the cubic phase predominates ($x \geq 0.75$). With the inclusion of BFN into BNBT matrix, the phase transition temperature displaces towards the higher temperature and attain its maximum for the composition with $x = 0.75$. The room temperature dielectric constant (ε_{RT}) has its maximal value for the composition with $x = 0.50$ at 1 kHz. The colossal dielectric constant near $x = 0.50$ may be attributed to various factors namely the interaction of local permanent electric dipoles under an external alternating electric field, domain wall vibration, ionic polarization and increasing grain size.

References

1. E. Cross, "Lead-free at last", *Nature*, **432** (2004) (2014) 24–25.
2. M.K.S. Bhutta, A. Omar, X. Yang, "Electronic waste: a growing concern in today's environment", *Econom. Res. Int.*, **2011** (2011) 474230.
3. Z. Wang, X.M. Chen, L. Ni, Y.Y. Liu, X.Q. Liu, "Dielectric relaxations in Ba(Fe$_{1/2}$Ta$_{1/2}$)O$_3$ giant dielectric constant ceramics", *Appl. Phys. Lett.*, **90** (2007) 102905–3.
4. I.P. Raevski, S.A. Prosandeev, A.S. Bogatin, M.A. Malitskaya, L. Jastrabik, "High dielectric permittivity in AFe$_{1/2}$B$_{1/2}$O$_3$ nonferroelectric perovskite ceramics (A = Ba, Sr, Ca; B = Nb, Ta, Sb)", *J. Appl. Phys.*, **93** (2003) 4130–4136.
5. C.Y. Chung, Y.H. Chang, G.J. Chen, "Effects of lanthanum doping on the dielectric properties of Ba(Fe$_{0.5}$Nb$_{0.5}$)O$_3$ ceramic", *J. Appl. Phys.*, **96** (2004) 6624–6628.
6. C.C. Homes, T. Vogt, S.M. Shapiro, S. Wakimoto, "Optical response of high-dielectric-constant perovskite-related oxide", *Science*, **293** (2001) 673–676.
7. S. Bhagat, K. Prasad, "Structural and impedance spectroscopy analysis of Ba(Fe$_{1/2}$Nb$_{1/2}$)O$_3$ ceramic", *Phys. Status Solidi A*, **207** (2010) 1232–1239.
8. I.M. Reaney, J. Petzelt, V.V. Voitsekhovskii, F. Chu, N. Setter, "B-site order and infrared reflectivity in A(B'B'')O$_3$ complex perovskite ceramics", *J. Appl. Phys.*, **76** (1994) 2086–2092.
9. S. Saha, T. Sinha, "Structural and dielectric studies of BaFe$_{0.5}$Nb$_{0.5}$O$_3$", *J. Phys. Condens. Mat.*, **14** (2002) 249–258.
10. C.Y. Chung, Y.H. Chang, G.J. Chen, Y.L. Chai, "Preparation, structure and ferroelectric properties of Ba(Fe$_{0.5}$Nb$_{0.5}$)O$_3$ powders by sol-gel method", *J. Cryst. Growth*, **284** (2005) 100–107.
11. S. Eitssayeam, U. Intatha, K. Pengpat, T. Tunkasiri, "Preparation and characterization of barium iron niobate (BaFe$_{0.5}$Nb$_{0.5}$O$_3$) ceramics", *Curr. Appl. Phys.*, **6** (2006) 316–318.
12. U. Intatha, , S. Eitssayeam, K. Pengpat, K.J. MacKenzie, T. Tunkasiri, "Dielectric properties of low temperature sintered LiF doped BaFe$_{0.5}$Nb$_{0.5}$O$_3$", *Mater. Lett.*, **61** (2007) 196–200.
13. Z. Wang, X.M. Chen, L. Ni, X.Q. Liu, "Dielectric abnormities of complex perovskite Ba(Fe$_{1/2}$Nb$_{1/2}$)O$_3$ ceramics over broad temperature and frequency range", *Appl. Phys. Lett.*, **90** (2007) 022904–3.
14. U. Intatha, S. Eitssayeam, T. Tunkasiri, "Giant dielectric behavior of BaFe$_{0.5}$Nb$_{0.5}$O$_3$ perovskite ceramic", *Int. J. Mod. Phys. B*, **22** (2008) 4717–4723.
15. S. Ke, H. Huang, H. Fan, H.L.W. Chan, L.M. Zhou, "Colossal dielectric response in barium iron niobate ceramics obtained by different precursors", *Ceram. Int.*, **34** (2008) 1059–1062.

16. N. Charoenthai, R. Traiphol, G. Rujijanagul, "Microwave synthesis of barium iron niobate and dielectric properties", *Mater. Lett.*, **62** (2008) 4446–4448.

17. S. Eitssayeam, U. Intatha, K. Pengpat, G. Rujijanagul, P. Thavornyutikarn, T. Tunkasiri, "Ferroelectric and pyroelectric properties of $0.8PbZr_{0.52}Ti_{0.48}O_3$-$0.2BaFe_{0.5}Nb_{0.5}O_3$ ceramics", *Ferroelectrics*, **376** (2008) 116–121.

18. C.Y. Chung, Y.S. Chang, G.J. Chen, C.C. Chung, T.W. Huang, "Effects of bismuth doping on the dielectric properties of $Ba(Fe_{0.5}Nb_{0.5})O_3$ ceramic", *Solid State Commun.*, **145** (2008) 212–217.

19. S. Bhagat, K.A. Nath, K.P. Chandra, R.K. Singh, A.R. Kulkarni, K. Prasad, "The structural, electrical and magnetic properties of perovskite $(1-x)Ba(Fe_{1/2}Nb_{1/2})O_3$-$xBaTiO_3$ ceramics", *Adv. Mater. Lett.*, **5** (2014) 117–121.

20. I.P. Raevski, S.A. Kuropatkina, S.P. Kubrin, S.I. Raevskaya, V.V. Titov, D.A. Sarychev, M.A. Malitskaya, A.S. Bogatin, I.N. Zakharchenko, "Dielectric and Mössbauer studies of high-permittivity $Ba(Fe_{1/2}Nb_{1/2})O_3$ ceramics with cubic and monoclinic perovskite structures", *Ferroelectrics*, **379** (2009) 48–54.

21. H. Li, Z. Wang, Y. Wen, "Enhancement of giant dielectric response in $Ba(Fe_{0.5}Nb_{0.5})O_3$ ceramics by Al substitution", *Ferroelectrics*, **491** (2016) 27–34.

22. J. Rödel, W. Jo, K.T. Seifert, E.M. Anton, T. Granzow, D. Damjanovic, "Perspective on the development of lead-free piezoceramics", *J. Am. Ceram. Soc.*, **92** (2009) 1153–1177.

23. B.J. Chu, D.R. Chen, G.R. Li, Q.R. Yin, "Electrical properties of $Na_{1/2}Bi_{1/2}TiO_3$-$BaTiO_3$ ceramics", *J. Eur. Ceram. Soc.*, **22** (2002) 2115–2121.

24. T. Takenaka, H. Nagata, "Current status and prospects of lead-free piezoelectric ceramics", *J. Eur. Ceram. Soc.*, **25** (2005) 2693–2700.

25. T. Takenaka, K.-I. Maruyama, K. Sakata, "$(Bi_{1/2}Na_{1/2})TiO_3$-$BaTiO_3$ system for lead-free piezoelectric ceramics", *Jpn. J. Appl. Phys.*, **30** (1991) 2236–2239.

26. R. Ranjan, A. Dviwedi, "Structure and dielectric properties of $(Na_{0.5}Bi_{0.5})_{(1-x)}Ba_xTiO_3$: $0 \leq x \leq 0.10$", *Solid State Commun.*, **135** (2005) 394–399.

27. G. Li, S. Liu, F. Liao, S. Tian, X. Jing, J. Lin, Y. Uesu, K. Kohn, K. Saitoh, M. Terauchi, N. Di, "The structural and electric properties of the perovskite system $BaTiO_3$-$Ba(Fe_{1/2}Ta_{1/2})O_3$", *J. Solid State Chem.*, **177** (2004) 1695–1703.

28. E. Antonelli, M. Letonturier, J.C. M'Peko, A.C. Hernandes, "Microstructural, structural and dielectric properties of Er^{3+}-modified $BaTi_{0.85}Zr_{0.15}O_3$ ceramics", *J. Eur. Ceram. Soc.*, **29** (2009) 1449–1455.

29. R.A. Swalin, J. Arents, "Thermodynamics of solids", *J. Electrochem. Soc.*, **109** (1962) 308C–308C.

30. S.K. Roy, S. Chaudhuri, R.K. Kotnala, D.K. Singh, B.P. Singh, S.N. Singh, K.P. Chandra, K. Prasad, "Dielectric and Raman studies of $Ba_{0.06}(Na_{1/2}Bi_{1/2})_{0.94}TiO_3$-$NaNbO_3$ ceramics", *Mater. Sci. Pol.*, **34** (2016) 437–445.

31. F. Bahri, H. Khemakhem, M. Gargouri, A. Simon, R. von der Mühll, J. Ravez, "Dielectric and Raman studies on the solid solution $(1-x)BaTiO_3/xNaNbO_3$ ceramics", *Solid State Sci.*, **5** (2003) 1229–1234.

32. S.K. Roy, S.N. Singh, S.K. Mukherjee K. Prasad, "$Ba_{0.06}(Na_{1/2}Bi_{1/2})_{0.94}TiO_3$-$Ba(Fe_{1/2}Ta_{1/2})O_3$: Giant permittivity lead-free ceramics", *J. Mater. Sci.: Mater. Electron.*, **28** (2017) 4763–4771.

33. T. Nakamura, S. Nomura, "Dielectric properties in $BaTiO_3$-$BaSnO_3$ and $BaTiO_3$-$Ba(Fe_{1/2}Ta_{1/2})O_3$ systems", *Jpn. J. Appl. Phys.*, **5** (1966) 1191–1196.

34. V. Isupov, "Phenomena at transformation from sharp to diffuse ferroelectric phase transition", *Ferroelectrics*, **143** (1993) 109–115.

35. L. Dong, D.S. Stone, R.S. Lakes, "Enhanced dielectric and piezoelectric properties of $xBaZrO_3$-$(1-x)BaTiO_3$ ceramics", *J. Appl. Phys.*, **111** (2012) 084107–10.

36. S. Lin, T. Lu, C. Jin, X. Wang, "Size effect on the dielectric properties of $BaTiO_3$ nanoceramics in a modified Ginsburg-Landau-Devonshire thermodynamic theory", *Phys. Rev. B*, **74** (2006) 134115–5.